

Dynamical interplay of disc thickness and the interstellar gas: implication for the longevity of spiral density waves

Soumavo Ghosh^{1,2} * and Chanda J. Jog³ **

¹ Max-Planck-Institut für Astronomie, Königstuhl 17, D-69117 Heidelberg, Germany

² Indian Institute of Astrophysics, Koramangala II Block, Bengaluru 560034, India

³ Department of Physics, Indian Institute of Science, Bangalore 560012, India

Received XXX; accepted YYY

ABSTRACT

A typical galactic disc has a finite thickness and in addition to stars it also contains a finite amount of interstellar gas. Here, we investigate the physical impact of the finite thickness of a galactic disc on the disc stability against the non-axisymmetric perturbations and on the longevity of the spiral density waves, with and without the presence of gas. The longevity is quantified via group velocity of density wavepackets. The galactic disc is first modelled as a collisionless stellar disc with finite height and then more realistically as a gravitationally-coupled stars plus gas system (with different thickness for stars and gas). For each case, we derive the appropriate dispersion relation in the WKB approximation, and study the dynamical effect of the disc thickness on the life-time of spiral density waves via a parametric approach. We find the generic trend that the effective reduction in disc self-gravity due to disc thickness makes it more stable against the non-axisymmetric perturbations, and shortens the life-span of the spiral density waves. Further, the interstellar gas and the disc thickness are shown to have a mutually opposite dynamical effect on the disc stability as well as the longevity of the spiral density waves. While the gas supports the non-axisymmetric features for a longer time, the disc thickness has an opposite, quenching effect. Consequently, the net change is set by the relative dominance of the opposite effects of the interstellar gas and the disc thickness.

Key words. galaxies: evolution - galaxies: kinematics and dynamics - galaxies: spiral - galaxies: structure - instabilities - hydrodynamics

1. Introduction

Spiral features are one of the most common non-axisymmetric structures (apart from a bar) in disc galaxies in the local Universe (e.g. Elmegreen et al. 2011; Yu et al. 2018; Savchenko et al. 2020). The occurrence of spiral structure in high-redshift (up to $z \sim 1.8$) disc galaxies is also known observationally (e.g. Elmegreen & Elmegreen 2014; Willett et al. 2017; Hodge et al. 2019). Simultaneous occurrence of spiral structure with an $m = 2$ bar or an $m = 1$ lopsidedness in disc galaxies is commonplace (e.g., see Rix & Zaritsky 1995; Bournaud et al. 2005; Buta et al. 2010; Zaritsky et al. 2013; Kruk et al. 2018; Ghosh et al. 2021). The Milky Way is a barred spiral galaxy (Weinberg 1992; Gerhard 2002) as well. In the past, a plethora of physical mechanisms ranging from bar-induced spirals (e.g., Salo et al. 2010), or due to tidal encounters (e.g., Toomre & Toomre 1972; Dobbs et al. 2010), or swing amplification of noise (Goldreich & Lynden-Bell 1965; Julian & Toomre 1966; Toomre 1981), due to disc response to giant molecular clouds (D’Onghia et al. 2013), due to interactions with other spirals (Masset & Tagger 1997), and due to recurrent groove modes (Sellwood & Lin 1989; Sellwood 2012; Sellwood & Carlberg 2019) to manifold-driven spirals (Athanassoula 2012), have been proposed for exciting spirals in disc galaxies.

Regardless of the physical mechanism(s) triggering the spiral instability in the disc, it is vital to address the *nature* and the longevity of spirals. Past studies of Goldreich & Lynden-Bell

(1965); Julian & Toomre (1966); Toomre (1981) proposed the spiral arms as transient *material arms* arising due to joint effects of epicyclic motion of stars, shear due to differential rotation, and the disc self-gravity. On the other hand, another set of studies by Lin & Shu (1964, 1966) envisaged the spirals as *quasi-stationary density waves* which rotate with respect to the disc with a well-defined pattern speed (for a detailed recent review, see Shu 2016). Implicit to the formalism of swing amplification, the material arms do not last for a long time (beyond a few dynamical timescales or a few $\times 10^8$ yr), and get wound up due to the disc differential rotation, whereas by definition, the spiral density waves are assumed to be stationary or they last forever. However, Toomre (1969) showed that, due to the radial group transport, a wavepacket made of such density waves eventually gets destroyed within ~ 1 Gyr time-scale, thereby posing a challenge to the *stationary* picture of the density wave theory. Spirals, generated in N -body simulations, are almost always found to be a transient phenomenon (e. g., see Sellwood 2011; Grand et al. 2012; Baba et al. 2013, for a review the reader is referred to Dobbs & Baba (2014)). However, a high-resolution N -body simulation by D’Onghia et al. (2013) showed that the spirals can sustain (at least in the statistical sense) for much longer time-scale due to the *non-linear* disc response to the perturbation caused by giant molecular cloud-like mass concentration. Another recent work by Saha & Elmegreen (2016) showed that bulges play a pivotal role in the sustenance of spirals in N -body simulations, and intermediate-sized bulges can help the spiral density wave to last longer (~ 5 Gyr) by providing a high Toomre Q -barrier in the inner region. Interstellar gas is shown to play a pivotal

* E-mail: ghosh@mpia-hd.mpg.de

** E-mail: cjog@iisc.ac.in

role too in the longevity of spiral density waves in disc galaxies. Earlier work by Sellwood & Carlberg (1984) demonstrated the role of a dissipative component in cooling the stellar disc and facilitating the generation of fresh spiral waves. Jog (1992) included gas along with stars in the framework of swing amplification mechanism for a more realistic treatment which yielded broad stellar arms as observed. Further, Ghosh & Jog (2015, 2016) showed that the interstellar gas helps spiral density waves to survive for a longer time (several billion years).

Most of the past analytical studies of spiral structure in disc galaxies treated the galactic disc as being *infinitesimally-thin*, for simplicity (but see Goldreich & Lynden-Bell 1965). This assumption is valid when the height of the disc is small as compared to the wavelength of the perturbation (see discussions in Toomre 1964; Binney & Tremaine 2008). However, in reality, a galactic disc has a finite height. López-Corredoira & Molgó (2014) showed that the Galactic disc flares substantially between Galactocentric radii 8 kpc to 25 kpc (also see Li et al. 2019) with the thin-disc component having a scale-height of ~ 300 pc in the Solar neighbourhood (e. g., see Jurić et al. 2008). This flaring of galactic disc (i.e., increment of scale-height) is a generic phenomenon (e.g., see de Grijs & Peletier 1997; Narayan & Jog 2002a; Sarkar & Jog 2019; García de la Cruz et al. 2021). In addition, the existence of a thick-disc component is now well-established observationally in both, external galaxies, as well as the Milky Way (e.g., see Tsikoudi 1979; Burstein 1979; Yoachim & Dalcanton 2006; Comerón et al. 2011a,b, 2018). Spirals play a pivotal dynamical role in disc dynamics by transporting angular momentum (Lynden-Bell & Kalnajs 1972); by causing radial migration of stars without heating (Sellwood & Binney 2002; Roškar et al. 2008; Schönrich & Binney 2009), and by exciting vertical breathing motions (Debattista 2014; Faure et al. 2014; Ghosh et al. 2020). Thus, a more realistic study of the spiral structure in disc galaxies should take into account the finite thickness of the disc.

Past theoretical studies have shown that the introduction of a finite thickness of a galactic disc results in a net reduction in the radial force in the mid-plane (e.g., see Toomre 1964; Jog & Solomon 1984; Jog 2014). This, in turn, facilitates the galactic disc to become more stable against the axisymmetric perturbations (Toomre 1964; Jog & Solomon 1984). Julian & Toomre (1966) demonstrated that the finite thickness of the stellar disc decreases the amplitude of the density transforms, in a local patch of the disc. Further, Ghosh & Jog (2018) showed the generic trend of suppressing the growth of the *swing-amplified* spirals due to the introduction of a finite thickness for the disc. However, little is known about the plausible role of the disc finite thickness on the radial group transport and the longevity of spiral density wave.

In this paper, we investigate the physical effect of the finite thickness of a galactic disc on the persistence of spiral density wave, both in absence and in presence of the interstellar gas. To achieve that, we first derive the appropriate dispersion relation in the WKB (Wentzel-Kramers-Brillouin) limit, for a collisionless stellar disc with a finite thickness and for a gravitationally-coupled two-component (stars plus gas) system with different thickness for the stellar and gas discs. Then, we systematically vary different input parameters, namely, the Toomre Q parameter, thickness of the disc, and the gas fraction, to check the dependence of the longevity of the spiral density wave, if any, on the finite thickness of the disc. The rest of the paper is organised as follows: Sect. 2 provides the derivation of the relevant dispersion relations in the WKB limit whereas Sect. 3 presents the dimensionless form of the corresponding dispersion relations. Sect. 4

gives our results covering the effect of finite thickness on the persistence of the spiral density waves, with and without the interstellar gas. Sects. 5 and 6 contain discussion and the main findings of this work, respectively.

2. WKB dispersion relation for galactic disc with finite thickness

Here, we first derive the dispersion relation for a one-fluid disc, and then extend to a collisionless stellar disc with finite height (Sects. 2.1–2.2). Finally, we consider a more realistic gravitationally-coupled two-component (stars plus gas) system where the stellar and the gaseous discs can have different scale-heights (Sect. 2.3), as observed in real galaxies. The underlying disc is taken to be axisymmetric and the spiral structure is treated as only a small perturbation on the steady-state axisymmetric disc, so that linear perturbation approach will be valid (for details see Binney & Tremaine 2008). A cylindrical coordinate system (R, ϕ, z) is used throughout the formulation.

2.1. One-component fluid disc

Following the treatment given in Binney & Tremaine (2008), we start with an *infinitesimally* thin fluid disc, and then we modify the formulation by introducing the effect due to the finite thickness of the fluid disc. The fluid disc is characterised by the disc surface density Σ_d and the sound speed c . We assume that the pressure acts only in the disc plane. Now, for such a system, the Euler's equations of motion in the cylindrical coordinates become

$$\frac{\partial v_R}{\partial t} + v_R \frac{\partial v_R}{\partial R} + \frac{v_\phi}{R} \frac{\partial v_R}{\partial \phi} - \frac{v_\phi^2}{R} = - \left(\frac{\partial(\Phi + \mathcal{H})}{\partial R} \right)_{z=0}, \quad (1)$$

and,

$$\frac{\partial v_\phi}{\partial t} + v_R \frac{\partial v_\phi}{\partial R} + \frac{v_\phi}{R} \frac{\partial v_\phi}{\partial \phi} + \frac{v_R v_\phi}{R} = - \frac{1}{R} \left(\frac{\partial(\Phi + \mathcal{H})}{\partial \phi} \right)_{z=0}. \quad (2)$$

Here, \mathcal{H} is the specific enthalpy of a polytropic fluid with an equation of state $p = K \Sigma_d^\gamma$ where $\gamma = (n + 1)/n$, n being the polytropic index, and K being a proportionality constant, and the form of \mathcal{H} is given by (Binney & Tremaine 2008)

$$\mathcal{H} = \frac{\gamma}{\gamma - 1} K \Sigma_d^{\gamma-1}. \quad (3)$$

Now, assuming the spiral density wave to be a small perturbation, we write $v_R = v_{R1}$; $v_\phi = v_{\phi 0} + v_{\phi 1}$, where v_{R1} and $v_{\phi 1}$ are small perturbations. Further assuming the random motion to be small compared to the rotation, from the Euler equation, it can be seen that the unperturbed motion gives rise to

$$v_{\phi 0} = \sqrt{R \frac{d\Phi_0}{dR}} = R\Omega(R), \quad (4)$$

where Φ_0 is the unperturbed potential and $\Omega(R)$ is the circular frequency. The linear perturbed equations of motion become

$$\frac{\partial v_{R1}}{\partial t} + \Omega \frac{\partial v_{R1}}{\partial \phi} - 2\Omega(R)v_{\phi 1} = - \left(\frac{\partial(\Phi_1 + \mathcal{H}_1)}{\partial R} \right)_{z=0}, \quad (5)$$

and,

$$\frac{\partial v_{\phi_1}}{\partial t} + \left[\frac{d(\Omega R)}{dR} + \Omega \right] v_{R_1} + \Omega \frac{\partial v_{\phi_1}}{\partial \phi} = -\frac{1}{R} \left(\frac{\partial(\Phi_1 + \mathcal{H}_1)}{\partial \phi} \right)_{z=0}, \quad (6)$$

where \mathcal{H}_1 is the perturbed specific enthalpy.

2.1.1. Introduction of finite thickness of the fluid disc

For simplicity, we assume that the disc has a constant density that does not vary with z , and the disc has a total thickness of $2h$. For an infinitesimally thin, axisymmetric disc, and an axisymmetric perturbation, the solution of the Poisson equation is given by (Toomre 1964)

$$\Phi_1 = -(2\pi G/|k|)\Sigma_1 \exp(-k|z|), \quad (7)$$

where k is the wavenumber of perturbation and Φ_1 and Σ_1 are the perturbation (or imposed) potential and the corresponding surface density, respectively. The perturbation surface density is taken to have the form $\exp[i(kr - \omega t)]$. For such a disc, the radial force at the mid-plane ($z = 0$) due to a vertical layer between z and $z + dz$ is proportional to $\exp[-k|z|dz]$. Hence, the net radial force at $z = 0$ is obtained by integrating over z to be (see Toomre 1964)

$$\left(\frac{\partial \Phi_1}{\partial R} \right)_{z=0} = -i2\pi G \Sigma_1 \delta, \quad (8)$$

where δ is the reduction factor which denotes the reduction in the radial force at the mid-plane due to the finite height for a constant density disc. This can also be thought of as a reduction in the disc surface density, and its form is given as (Toomre 1964)

$$\delta = [1 - \exp(-kh)]/kh. \quad (9)$$

In an analogous fashion, by integrating the contribution of force due to layers at different z , we can show that the azimuthal force in the mid-plane is also reduced by an identical reduction factor.

We point out that, the perturbation potential and the surface density in the framework of WKB approximation, follow the same relation (Eq. (7)) as above (see Eqs. (6)-(18) in Binney & Tremaine 2008). Hence, a similar analysis (as mentioned above) will yield a same reduction factor δ (Eq. (9)) in the radial, as well as the azimuthal force at mid-plane, for the WKB approximation as well. Therefore, in case of a fluid disc with a finite thickness, Eqs. (5) and (6) become

$$\frac{\partial v_{R_1}}{\partial t} + \Omega \frac{\partial v_{R_1}}{\partial \phi} - 2\Omega(R)v_{\phi_1} = -\left(\frac{\partial \Phi_1}{\partial R} \delta + \frac{\partial \mathcal{H}_1}{\partial R} \right)_{z=0}, \quad (10)$$

and,

$$\frac{\partial v_{\phi_1}}{\partial t} + \left[\frac{d(\Omega R)}{dR} + \Omega \right] v_{R_1} + \Omega \frac{\partial v_{\phi_1}}{\partial \phi} = -\frac{1}{R} \left(\frac{\partial \Phi_1}{\partial \phi} \delta + \frac{\partial \mathcal{H}_1}{\partial \phi} \right)_{z=0}. \quad (11)$$

We assume the trial solutions are of the form

$$\begin{aligned} v_{R_1} &= Re \left[v_{R_a}(R) e^{i(m\phi + kR - \omega t)} \right] \\ v_{\phi_1} &= Re \left[v_{\phi_a}(R) e^{i(m\phi + kR - \omega t)} \right] \\ \Phi_1 &= Re \left[\Phi_a(R) e^{i(m\phi + kR - \omega t) - k|z|} \right] \\ \Sigma_{d_1} &= Re \left[\Sigma_{d_a}(R) e^{i(m\phi + kR - \omega t)} \right] \\ \mathcal{H}_1 &= Re \left[\mathcal{H}_a(R) e^{i(m\phi + kR - \omega t)} \right]. \end{aligned} \quad (12)$$

Putting these in Eqs. (10) and (11), and after some algebraic simplification we get,

$$v_{R_a} = \frac{i}{\Delta} \left[(\omega - m\Omega) \left(\delta \frac{d\Phi_a}{dR} + \frac{d\mathcal{H}_a}{dR} \right) - \frac{2m\Omega}{R} (\Phi_a \delta + \mathcal{H}_a) \right], \quad (13)$$

and,

$$v_{\phi_a} = -\frac{1}{\Delta} \left[2B \left(\delta \frac{d\Phi_a}{dR} + \frac{d\mathcal{H}_a}{dR} \right) + \frac{m(\omega - m\Omega)}{R} (\Phi_a \delta + \mathcal{H}_a) \right], \quad (14)$$

where B is the Oort constant and $\Delta \equiv \kappa^2 - (\omega - m\Omega)^2$, κ being the epicyclic frequency. Also, the perturbed equation of state gives $\mathcal{H}_a = c^2 \frac{\Sigma_{d_a}}{\Sigma_0}$, where Σ_0 is the unperturbed disc surface density (for details see Binney & Tremaine 2008).

Similarly, the perturbed continuity equation in cylindrical coordinates is

$$\frac{\partial \Sigma_{d_1}}{\partial t} + \Omega \frac{\partial \Sigma_{d_1}}{\partial \phi} + \frac{1}{R} \frac{\partial}{\partial R} (R v_{R_1} \Sigma_0) + \frac{\Sigma_0}{R} \frac{\partial v_{\phi_1}}{\partial \phi} = 0, \quad (15)$$

which, after substituting the trial solution (Eq. (12)) becomes

$$-i(\omega - m\Omega)\Sigma_{d_a} e^{ikR} + \frac{1}{R} \frac{d}{dR} (R v_{R_a} e^{ikR} \Sigma_0) + \frac{im\Sigma_0}{R} v_{\phi_a} e^{ikR} = 0. \quad (16)$$

2.1.2. Dispersion relation

Now, we invoke the WKB approximation to derive an analytical dispersion relation. In this limit, Eqs. (13)-(14) reduce to (for details, see Binney & Tremaine 2008)

$$v_{R_a} = -\frac{(\omega - m\Omega)}{\Delta} k (\Phi_a \delta + \mathcal{H}_a) \quad \text{and} \quad v_{\phi_a} = -\frac{2iB}{\Delta} k (\Phi_a \delta + \mathcal{H}_a), \quad (17)$$

Also, the continuity equation (Eq. (16)) reduces to

$$-(\omega - m\Omega)\Sigma_{d_a} + k\Sigma_0 v_{R_a} = 0, \quad (18)$$

as in the WKB approximation, the last term in Eq. (16) involving v_{ϕ_a} is smaller than the first two terms and can be dropped (Binney & Tremaine 2008). Now, on substituting the values for v_{R_a} , \mathcal{H}_a as obtained above and $\Phi_a = -2\pi G \Sigma_a / |k|$, as obtained in the WKB limit using Eqs. (7) and (12), where Φ_a and Σ_a are the imposed perturbation potential and the corresponding imposed

perturbation surface density; and after some algebraic manipulation, Eq. (18) reduces to

$$\Sigma_{d_a} = \frac{2\pi G|k|\Sigma_0\delta}{\kappa^2 - (\omega - m\Omega)^2 + c^2k^2} \Sigma_a, \quad (19)$$

where Σ_{d_a} is the disc response density. Now, for a *self-sustained* density wave, the quantities Σ_a and Σ_{d_a} should be equal, and hence the dispersion relation becomes (Binney & Tremaine 2008)

$$(\omega - m\Omega)^2 = \kappa^2 - 2\pi G|k|\Sigma_0\delta + c^2k^2, \quad (20)$$

where m is a positive integer, denoting the m -fold rotational symmetry of the perturbation. We note that, in the limit of $h \rightarrow 0$, so that $\delta \rightarrow 1$, the dispersion relation (Eq. (20)) reduces to the corresponding dispersion relation for an infinitesimally-thin fluid disc (see Binney & Tremaine 2008), as expected. In other words, Eq. (20) is a generalisation of the dispersion relation for an infinitesimally thin fluid disc. Here, the additional factor δ comes in from the inclusion of the effect of finite height in the calculation.

2.2. One-component stellar disc

A *cold* stellar disc is dynamically equivalent to a fluid disc with zero pressure or zero enthalpy, and hence, the perturbation \bar{v}_{R_1} in the mean radial velocity of the stars can be obtained from Eqs. (5) and (6) (assuming zero pressure) as (Binney & Tremaine 2008)

$$\bar{v}_{R_a} = -\frac{\omega - m\Omega}{\Delta} k\Phi_a. \quad (21)$$

where Δ is as defined earlier. If we assume the disc to have a finite thickness of $2h$ and a constant density ρ (as in Sect. 2.1.1), then in an analogous fashion, the radial force in the mid-plane is reduced by a reduction factor δ (defined in Eq. (9)). Then following the same procedure as done in Sect. 2.1.1, namely solving the Euler equation (Eq. 10) with zero enthalpy, the solution for \bar{v}_{R_a} is obtained in the WKB limit to be

$$\bar{v}_{R_a} = -\frac{\omega - m\Omega}{\Delta} k(\Phi_a \delta). \quad (22)$$

As expected, this can be obtained from Eq. (17) by setting the enthalpy to be zero.

Now, if the stellar disc is not sufficiently *cold*, i.e., if the typical epicyclic amplitude is not small enough as compared to the wavelength ($2\pi/k$) of perturbation, then the net response velocity measured at a given location is due to stars with large epicyclic amplitudes and hence would have sampled different values of the spiral potential. This results in a partial cancellation in the mean velocity perturbation response to the imposed potential (for details see Binney & Tremaine 2008). Therefore, the resulting expression for the mean velocity perturbation for a thin disc is given by

$$\bar{v}_{R_a} = -\frac{\omega - m\Omega}{\Delta} k\Phi_a \mathcal{F}, \quad (23)$$

where \mathcal{F} is the factor by which the response of the disc to a given spiral perturbation is diminished below the value for a cold disc. The form of \mathcal{F} is discussed later in Sect. 3.2.

Now, it is straightforward to show that, for a stellar disc with finite thickness, where we start with \bar{v}_{R_a} as for a finite height case above (Eq. (22)), and then taking account of the reduction in the collisionless disc response when the disc is not cold, then these two effects manifest simultaneously and the expression for the mean velocity perturbation becomes

$$\bar{v}_{R_a} = -\frac{\omega - m\Omega}{\Delta} k(\Phi_a \delta) \mathcal{F}. \quad (24)$$

Also, the perturbed continuity equation in the WKB limit becomes (see e.g., Binney & Tremaine 2008)

$$-(\omega - m\Omega)\Sigma_{d_a} + k\Sigma_0\bar{v}_{R_a} = 0. \quad (25)$$

Note that this is identical to Eq. (18) since the continuity equation has the same form for fluid and collisionless cases. On substituting \bar{v}_{R_a} from Eq. (24), the above reduces to

$$-(\omega - m\Omega)\Sigma_{d_a} + k\Sigma_0 \left[-\frac{\omega - m\Omega}{\Delta} k(\Phi_a \delta) \mathcal{F} \right] = 0. \quad (26)$$

Finally, invoking the WKB approximation as before (Sect. 2.1.1), we substitute $\Phi_a = -2\pi G\Sigma_a/|k|$ (Sect. 2.2), and obtain

$$\Sigma_{d_a} = \frac{2\pi G\Sigma_0|k|}{\Delta} \delta \mathcal{F} \Sigma_a. \quad (27)$$

Again, for a self-sustained density wave, the disc response surface density (Σ_{d_a}) should be equal to the imposed surface density (Σ_a). This, in turn, yields the dispersion relation for the collisionless disc in the WKB limit as

$$(\omega - m\Omega)^2 = \kappa^2 - 2\pi G|k|\Sigma_0\delta \mathcal{F}. \quad (28)$$

Here also we note that in the limit of $h \rightarrow 0$, so that $\delta \rightarrow 1$, the dispersion relation (Eq. (28)) reduces to the corresponding dispersion relation for an infinitesimally-thin collisionless stellar disc (see Binney & Tremaine 2008), as expected. In other words, Eq. (28) is a generalisation of the dispersion relation for an infinitesimally-thin stellar disc. Here, the additional factor δ comes in from the inclusion of the effect of finite height in the calculation.

2.3. Two-component star-gas system with different finite thickness

Here, we treat a galactic disc as a gravitationally coupled two-component (stars plus gas) system¹. The stellar disc is taken to be collisionless in nature and is characterised by a surface density Σ_{0s} , a one-dimensional velocity dispersion, σ_s , and a total thickness of $2h_s$, while the gas disc is treated as a fluid and is characterised by the surface density Σ_{0g} , a one-dimensional velocity dispersion or the sound speed, c_g , and a total thickness of $2h_g$. Since the stars and the gas are gravitationally-coupled, therefore, their motion will be governed by the joint potential (Φ_{tot}) which is set by both the stellar and the gas discs, i.e., $\Phi_{\text{tot}} = \Phi_s + \Phi_g$. The right hand side of Eqs. (1) and (2) will now

¹ The main difference between this work with that presented in Ghosh & Jog (2015) is that here we take into account the finite thickness of both the stellar and the gaseous discs.

contain a derivative of the total potential. Thus, the steady-state unperturbed motion will now be given by

$$v_{\phi 0i} = \sqrt{R \frac{d\Phi_{\text{tot},0}}{dR}} = R\Omega(R). \quad (29)$$

Now, for such a system, the reduction due to the finite height affects the corresponding radial force of each component separately, and each component is affected by the net force due to both components (see e.g. Jog & Solomon 1984). Hence, the R.H.S. of the perturbed Euler equation (Eq. (10)) becomes $(\partial\Phi_{s1}/\partial R)\delta_s + (\partial\Phi_{g1}/\partial R)\delta_g + (\partial\mathcal{H}_{1g}/\partial R)$ for $i = g$ (gas), while for the collisionless stellar disc ($i = s$), only the first two terms above (without the enthalpy term) are kept, as discussed in Sect. 2.2. The same correction applies to the azimuthal perturbed equation of motion as well. Now assuming trial solutions similar to those as shown in Eq. (12), and invoking the WKB approximation, the solutions of the Euler equations give the amplitudes of perturbed velocity along the radial and the azimuthal directions for the stellar and the gas disc respectively as

$$\begin{aligned} v_{R_{as}} &= -\frac{(\omega - m\Omega)}{\Delta} k(\Phi_{as}\delta_1\mathcal{F} + \Phi_{ag}\delta_g) \\ v_{\phi_{as}} &= -\frac{2iB}{\Delta} k(\Phi_{as}\delta_1\mathcal{F} + \Phi_{ag}\delta_g), \end{aligned} \quad (30)$$

and,

$$\begin{aligned} v_{R_{ag}} &= -\frac{(\omega - m\Omega)}{\Delta} k(\Phi_{as}\delta_s + \Phi_{ag}\delta_g + \mathcal{H}_{ag}) \\ v_{\phi_{ag}} &= -\frac{2iB}{\Delta} k(\Phi_{as}\delta_s + \Phi_{ag}\delta_g + \mathcal{H}_{ag}). \end{aligned} \quad (31)$$

Substituting the expression for $v_{R_{as}}$ from Eq. (30) in the perturbed continuity equation (analog of Eq. (25)), we get

$$\Sigma_{d_{as}} [\kappa^2 - (\omega - m\Omega)^2] = k\Sigma_{0s} [k(\Phi_{as}\delta_1\mathcal{F} + \Phi_{ag}\delta_g)]. \quad (32)$$

On substituting the expression for the perturbation potentials in terms of the surface densities in the WKB limit, namely $\Phi_{as} = -2\pi G\Sigma_{as}/|k|$ and similarly for Φ_{ag} , and setting Σ_{as} , the imposed or perturbation stellar surface density equal to $\Sigma_{d_{as}}$, the stellar response surface density for a self-consistent solution, the above reduces to

$$\frac{\Sigma_{d_{as}}}{\Sigma_{ag}} = \frac{2\pi Gk\Sigma_{0s}\delta_g}{(\kappa^2 - (\omega - m\Omega)^2 - 2\pi G|k|\Sigma_{0s}\delta_s\mathcal{F})}. \quad (33)$$

Similarly for the gas disc, the continuity equation (Eq. (18)) combined with the perturbed velocity component in the WKB limit (Eq. (31)) gives:

$$\Sigma_{d_{ag}} [\kappa^2 - (\omega - m\Omega)^2] = k\Sigma_{0g} [k(\Phi_{as}\delta_s + \Phi_{ag}\delta_g + \mathcal{H}_{ag})]. \quad (34)$$

On substituting the expression for the perturbation potentials in terms of the surface densities in the WKB limit, namely $\Phi_{as} = -2\pi G\Sigma_{as}/|k|$ and similarly for Φ_{ag} ; and further for self-consistency setting $\Sigma_{ag} = \Sigma_{d_{ag}}$, the above equation reduces to

$$\frac{\Sigma_{as}}{\Sigma_{d_{ag}}} = \frac{(\kappa^2 - (\omega - m\Omega)^2 + k^2c_g^2 - 2\pi G|k|\Sigma_{0g}\delta_g)}{2\pi Gk\Sigma_{0g}\delta_s}. \quad (35)$$

Combining Eqs. (33) and (35) and setting the condition of self-consistency ($\Sigma_{as} = \Sigma_{d_{as}}$ and similarly for the gas disc), we get the dispersion relation for this joint star-gas system as

$$\frac{2\pi G\Sigma_{0s}|k|\delta_s\mathcal{F}\left(\frac{\omega - m\Omega}{\kappa}, \frac{k^2\sigma_s^2}{\kappa^2}\right)}{\kappa^2 - (\omega - m\Omega)^2} + \frac{2\pi G\Sigma_{0g}\delta_g|k|}{\kappa^2 - (\omega - m\Omega)^2 + c_g^2k^2} = 1. \quad (36)$$

We checked that for an infinitesimally thin disc (where the reduction factors $\delta_i \rightarrow 1$ ($i = s, g$), see Eq. (9)), the above reduces to the dispersion relation for a star-gas case obtained in Ghosh & Jog (2015), as expected.

We next define

$$\begin{aligned} \alpha_s &= \kappa^2 - 2\pi G\Sigma_{0s}\delta_s|k|\mathcal{F}\left(\frac{\omega - m\Omega}{\kappa}, \frac{k^2\sigma_s^2}{\kappa^2}\right) \\ \alpha_g &= \kappa^2 - 2\pi G\Sigma_{0g}\delta_g|k| + k^2c_g^2 \\ \beta_s &= 2\pi G\Sigma_{0s}\delta_s|k|\mathcal{F}\left(\frac{\omega - m\Omega}{\kappa}, \frac{k^2\sigma_s^2}{\kappa^2}\right) \\ \beta_g &= 2\pi G\Sigma_{0g}\delta_g|k|. \end{aligned} \quad (37)$$

Upon substitution in Eq. (36) and after some algebraic simplification, we get

$$(\omega - m\Omega)^4 - (\alpha_s + \alpha_g)(\omega - m\Omega)^2 + (\alpha_s\alpha_g - \beta_s\beta_g) = 0. \quad (38)$$

This is a quadratic equation in $(\omega - m\Omega)^2$. Solving it we get

$$(\omega - m\Omega)^2 = \frac{1}{2} \left[(\alpha_s + \alpha_g) \pm \left\{ (\alpha_s + \alpha_g)^2 - 4(\alpha_s\alpha_g - \beta_s\beta_g) \right\}^{1/2} \right]. \quad (39)$$

The additive root for $(\omega - m\Omega)^2$ always leads to a positive quantity, hence it indicates always oscillatory perturbations under all conditions (same as for axisymmetric case; see Jog & Solomon 1984). In order to study the stability of the system and its further consequences, we therefore consider only the negative root which is

$$(\omega - m\Omega)^2 = \frac{1}{2} \left[(\alpha_s + \alpha_g) - \left\{ (\alpha_s + \alpha_g)^2 - 4(\alpha_s\alpha_g - \beta_s\beta_g) \right\}^{1/2} \right]. \quad (40)$$

We mention that, the underlying formalism, presented here, closely follows that presented in Jog & Solomon (1984). This builds on the treatment for one-component stellar and gas discs of finite height as in Sects. 2.1 and 2.2. On solving the coupled equations, the resulting dispersion relation is given by Eq. (36), which has the solution Eq. (40). Also, we caution the reader that the form for the solution of the dispersion relation (Eq. (40)) and the subsidiary variables α_s , α_g , β_s and β_g (Eq. (37)) (in terms of which Eq. (40) is written) may appear similar to that in Jog & Solomon (1984, which treated a two-fluid case), and Ghosh & Jog (2015, which treated a star-gas case where the effect of stellar dispersion was included in terms of the reduction factor \mathcal{F}). In fact these were defined to have a similar form by construction because all three are two-component formulations and have a similar underlying mathematical symmetry, but with different treatment for stars and gas, and the current work includes the effect of finite height.

3. Dimensionless form of dispersion relations in the WKB limit

In the literature, usually the dispersion relations are described in terms of some dimensionless quantities, for the sake of convenience. Here, we follow the same procedure for the dispersion relations derived in the previous sections.

3.1. One-component fluid disc with finite thickness

Dividing both sides of Eq. (20) by κ^2 , and after some algebraic simplification we get

$$s^2 = 1 - x\delta + \frac{1}{4}x^2Q^2, \quad (41)$$

where $s = (\omega - m\Omega)/\kappa$, and $x (= |k|/k_{\text{crit}})$ are the dimensionless frequency and wavenumber of the perturbation, respectively; and $k_{\text{crit}} (= \kappa^2/2\pi G\Sigma_0)$ is the largest stable wavenumber for a pressure-less stellar disc. $Q (= \kappa c/\pi G\Sigma_0)$ is the usual Toomre Q parameter for a fluid disc (Toomre 1964). Also, $|k|h$ can be expressed as $|k|h = (|k|/k_{\text{crit}}) \times (k_{\text{crit}}h) = x\beta$. Here, β is defined to be equal to $k_{\text{crit}} \times h$. Therefore, the dispersion relation becomes

$$s^2 = 1 - x\delta + \frac{1}{4}x^2Q^2, \quad (42)$$

where the form of δ reduces to

$$\delta = \frac{1 - \exp(-x\beta)}{x\beta}. \quad (43)$$

Now, the value of β is dependent on the chosen values of k_{crit} , i.e., for the same thickness of a disc, the values of β will be different depending on the values of k_{crit} . We note that in the Solar neighbourhood, a circular velocity (v_c) of $\sim 220 \text{ km s}^{-1}$ and $\Sigma \sim 45 \text{ M}_\odot \text{ pc}^{-2}$ (e.g. see Mera et al. 1998; Narayan & Jog 2002b) will produce $k_{\text{crit}} \sim 1 \text{ kpc}^{-1}$. However, recent studies have reported slightly different values for the circular velocity and the Solar position (e.g., see Gillessen et al. 2009; Schönrich et al. 2010; Schönrich 2012; McMillan et al. 2018; Schönrich et al. 2019). The Galactocentric distance of the Sun is 8.27 kpc (Schönrich 2012) which is in agreement with the other measurements (within their error-bars Gillessen et al. 2009; McMillan et al. 2018). Also, the circular velocity at the Solar radius is 237.8 km s^{-1} (Schönrich et al. 2010) which, in turn, gives circular frequency at the Solar radius as $28.8 \text{ km s}^{-1} \text{ kpc}^{-1}$. Assuming a flat rotation curve, the corresponding epicyclic frequency becomes $40.7 \text{ km s}^{-1} \text{ kpc}^{-1}$. We use these latest values of Ω and κ and consider the group transport at the solar neighbourhood ($R = 8.27 \text{ kpc}$) in the subsequent sections, unless stated otherwise. Using these recent values, we estimate $k_{\text{crit}} \sim 1.3 \text{ kpc}^{-1}$. Therefore, for the sake of uniformity, we chose $k_{\text{crit}} = 1.3 \text{ kpc}^{-1}$ for all cases considered here, unless stated otherwise. The resulting behaviour of the reduction factor δ is shown in Appendix A.

3.2. One-component stellar disc with finite thickness

Dividing both sides of Eq. (28) by κ^2 and after some algebraic simplification we get

$$s^2 = 1 - x\delta\mathcal{F}(s, \chi), \quad (44)$$

where, $\chi = k^2\sigma_s^2/\kappa^2 = 0.286Q_s^2x^2$, and δ is already given in Eq. (43). The form for \mathcal{F} for a razor-thin disc whose stellar equilibrium state is described by the Schwarzschild distribution function, is given by (Binney & Tremaine 2008):

$$\mathcal{F}(s, \chi) = \frac{2}{\chi} \exp(-\chi)(1 - s^2) \sum_{n=1}^{\infty} \frac{I_n(\chi)}{1 - s^2/n^2}, \quad (45)$$

where I_n is the modified Bessel function of first kind.

3.3. Two-component star-gas system with different finite thickness

Proceeding as before, on dividing both sides of Eq. (40) by κ^2 and after some algebraic simplification we get

$$s^2 = \frac{1}{2} \left[(\alpha'_s + \alpha'_g) - \left\{ (\alpha'_s + \alpha'_g)^2 - 4(\alpha'_s\alpha'_g - \beta'_s\beta'_g) \right\}^{1/2} \right], \quad (46)$$

where

$$\begin{aligned} \alpha'_s &= 1 - (1 - \epsilon)x\delta_s\mathcal{F}(s, \xi) \\ \alpha'_g &= 1 - \epsilon x\delta_g + \frac{1}{4}Q_g^2\epsilon^2x^2 \\ \beta'_s &= (1 - \epsilon)x\delta_s\mathcal{F}(s, \xi) \\ \beta'_g &= \epsilon x\delta_g \end{aligned} \quad (47)$$

where, $\xi = k^2\sigma_g^2/\kappa^2 = 0.286Q_g^2(1 - \epsilon)^2x^2$. The three dimensionless parameters Q_s , Q_g and ϵ are, respectively the Toomre Q parameters for stars $Q_s (= \kappa\sigma_s/(3.36G\Sigma_{0s}))$, and for gas $Q_g = (\kappa c_g/(\pi G\Sigma_{0g}))$ and, $\epsilon = \Sigma_{0g}/(\Sigma_{0s} + \Sigma_{0g})$ the gas mass fraction in the disc, respectively. Also, the forms of δ_i are given by

$$\delta_i = \frac{1 - \exp(-x\beta_i)}{x\beta_i}. \quad (48)$$

where $i = s, g$ for stars and gas, respectively. We note that, when the height $h_i \rightarrow 0$, and so $\delta_i \rightarrow 1$, Eq. (46) reduces to the dispersion relation for the gravitationally coupled two-component (stars plus gas) system which is infinitesimally thin (see Ghosh & Jog 2015), as expected.

4. Results

Here, we present the results related to the dynamical effect of inclusion of a finite thickness of the disc, with or without the presence of the interstellar gas on the disc stability and the longevity of a spiral density wave. For a bi-symmetric ($m = 2$) spiral density wave, the pattern speed $\Omega_p = \omega/2$ and $s = (\omega - 2\Omega)/\kappa = 2(\Omega_p - \Omega)/\kappa$. Here, $s = 0$ corresponds to the corotation (CR) point and $|s| = 1$ gives the Lindblad resonances (Ghosh & Jog 2016).

To quantify the disc stability, we define a quantity $|s|_{\text{cut-off}}$ as the lowest value of the dimensionless frequency (s), corresponding to an appropriate dispersion relation, for which one is able to obtain a real or stable wave solution at any given R (for details, see e.g., Binney & Tremaine 2008; Ghosh & Jog 2016). For s lying in the forbidden region namely, between the corotation or $s = 0$ and $s_{\text{cut-off}}$, the solution is imaginary and the wave is transient, at any given radius R (for details see discussions in Binney & Tremaine 2008; Ghosh & Jog 2016). In other words, the value of $|s|_{\text{cut-off}}$ denotes the edge of the forbidden region. A decrease in the value of $|s|_{\text{cut-off}}$ signifies the decrease in the forbidden

zone; this results in the disc becoming more prone to being unstable against the perturbations. Conversely, an increase in the value of $|s|_{\text{cut-off}}$ denotes the increase in the forbidden zone, and the disc becomes more stable against the perturbations.

As for the longevity of the spiral density wave, following Toomre (1969), we study the radial group transport of a wavepacket of such a density wave. To achieve that, we calculate the radial group velocity from the local dispersion relation, appropriate for a particular system considered here. It is known that the information from a disturbance, generated at a certain radius R , propagates in the disc with its group velocity v_g . When the medium is inhomogeneous, the group velocity, at a given radius R , is defined as (e. g., see Whitham 1960; Lighthill 1965)

$$v_g(R) = \frac{\partial \omega(k, R)}{\partial k}. \quad (49)$$

The value of the group velocity (v_g), at a given R , can be estimated from the slope of the local dispersion relation (when expressed in a dimensionless form) by using the following equation (e. g., see Toomre 1969; Binney & Tremaine 2008)

$$v_g(R) = \text{sgn}(ks) \left(\frac{\kappa}{k_{\text{crit}}} \right) \frac{ds}{dx}. \quad (50)$$

Here, s and x are the dimensionless frequency and the wavenumber of the perturbation, respectively, and $\text{sgn}(ks) = \pm 1$ depending on whether $ks > 0$ or $ks < 0$. Here, the slope is obtained at a point x where the observed value of s intersects the dispersion relation curve. Thus, the location (or the x value) where the slope is to be calculated is determined by the pattern speed (Ω_p) value as well as the underlying mass distribution (which in turn sets the values of Ω and κ), for more details see Sect. 4.1.

A decrease in the group velocity implies that a wavepacket of such density wave would take a longer time to reach the centre of the disc, and eventually get absorbed. In other words, a decrease in the group velocity signifies a longer persistence of the spiral density waves in the disc (for further discussions, see, e. g., Toomre 1969; Ghosh & Jog 2015). Sect. 4.1 provides the details of the effect of finite thickness on the disc instability and longevity of spiral density wave for the one-component stellar disc whereas Sect. 4.2 gives the same for the gravitationally-coupled two-component (stars plus gas) disc. We mention that the methodology of investigating the disc stability against the $m = 2$ spiral density wave is similar to that in Ghosh & Jog (2016) whereas the treatment for calculation of the group velocity is similar to that in Ghosh & Jog (2015), except here we use the appropriate dispersion relations for a one-component stellar disc, and a two-component disc with *finite height*, as derived in the previous section.

4.1. Effect of finite thickness on one-component stellar disc

To study the dynamical effect of the disc finite thickness, first we calculate the dispersion relation (Eq. (44)) for Toomre $Q = 1.1$ while varying the disc thickness, or equivalently β from 0.1 to 0.3. Fig. 1 shows the corresponding dispersion relations. For comparison, we also show the corresponding dispersion relation for an infinitesimally-thin stellar disc with $Q = 1.1$. Toomre (1969) assumed an $Q = 1$ which denotes the neutral stability of the stellar disc. Here, instead, we assume a slightly higher value of $Q = 1.1$ such that stellar disc is stable against axisymmetric perturbation, but the self-gravity is still important (for details, see Toomre 1964; Jog & Solomon 1984).

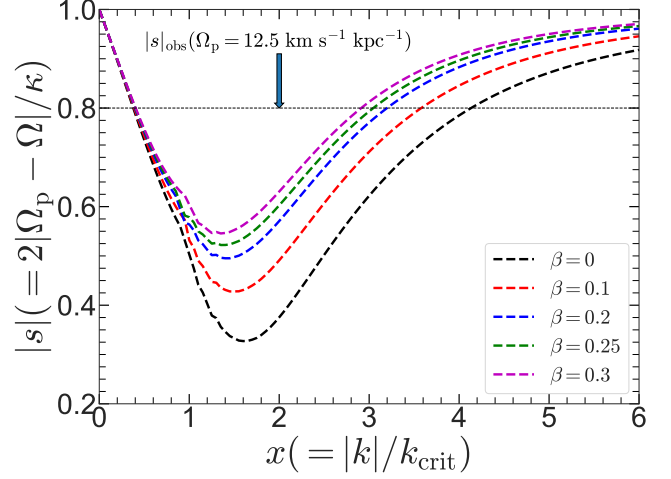


Fig. 1. Dispersion relation for the one-component stellar disc (Eq (44)) is shown for $Q = 1.1$ and for $\beta = 0.1$ – 0.3 . For comparison, the corresponding dispersion relation for the zero-thickness (or infinitesimally-thin) stellar disc is also shown (black dashed line). The horizontal dashed line (in black) denotes the $|s|_{\text{obs}}$ value (calculated at $R = 8.27$ kpc) corresponding to an assumed pattern speed of $12.5 \text{ km s}^{-1} \text{ kpc}^{-1}$.

4.1.1. Disc stability against spiral density waves

A visual inspection of Fig. 1 reveals that with increasing thickness of the disc, the $|s|_{\text{cut-off}}$ values increase steadily. This implies that the stellar disc becomes more and more stable against the non-axisymmetric perturbations. In order to study this more quantitatively, we calculate the $|s|_{\text{cut-off}}$ values from the dispersion relation while systematically varying the Toomre Q values from 1.1 to 2, and $\beta = 0.1, 0.3$, and 0.5 . The resulting variation of the $|s|_{\text{cut-off}}$ values for different β and Toomre Q parameter values are shown in Fig. 2. For reference, we also show the corresponding $|s|_{\text{cut-off}}$ values for a one-component stellar disc with zero thickness (i. e., $\beta = 0$). As seen clearly from Fig. 2, for a fixed Toomre Q parameter, the $|s|_{\text{cut-off}}$ value increases monotonically with increasing β values. Although this trend remains true for the whole range of Toomre Q values considered here, the effect of increase in the $|s|_{\text{cut-off}}$ value due to disc thickness is more prominent for lower Toomre Q values considered here. For example, for $Q = 1.1$, the $|s|_{\text{cut-off}}$ values increase almost by a factor of 2 on changing the β from 0 (zero-thickness) to 0.5 (~ 385 pc); whereas the corresponding change is much smaller, by $\sim 7\%$ for $Q = 2$. This trend is not surprising, since for lower values of Q , the disc self-gravity is more relevant, and consequently the reduction in the self-gravity (due to finite-thickness) will be more pronounced as compared to the case with a higher Toomre Q value. The physical implications of the increasing $|s|_{\text{cut-off}}$ value with thickness is discussed below.

4.1.2. Effect of finite thickness on the allowed range of pattern speed values

As the $|s|_{\text{cut-off}}$ value increases with increasing thickness, this implies that the forbidden region (i. e., the region between the CR and $|s|_{\text{cut-off}}$) also increases. In other words, introduction of a finite thickness of the disc helps to stabilise it against the non-axisymmetric perturbations. The increase in the $|s|_{\text{cut-off}}$ value with increasing thickness has far-reaching impact on the pattern

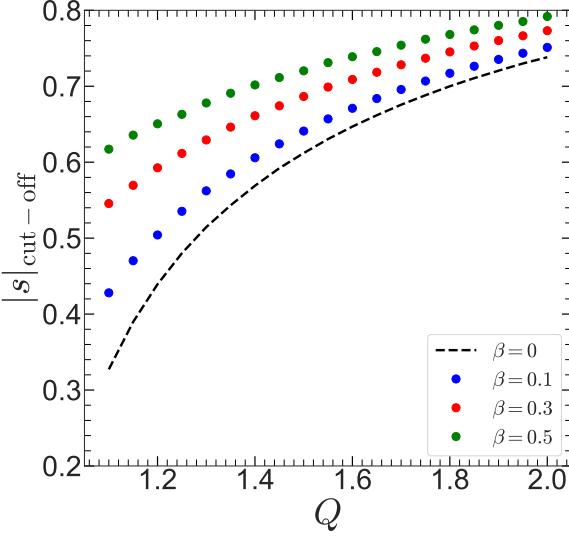


Fig. 2. One-component stellar disc: Variation of the $|s|_{\text{cut-off}}$ values as a function of the Toomre Q parameter are shown for different disc thickness (β). The black dashed line shows the corresponding $|s|_{\text{cut-off}}$ values for a one-component stellar disc which is infinitesimally-thin. For a fixed Toomre Q , the $|s|_{\text{cut-off}}$ values increase monotonically with β .

speed (Ω_p) value of a stable, spiral density wave. In a collisionless stellar disc, a spiral density wave exists only in those regions where

$$\Omega - \kappa/2 \leq \Omega_p \leq \Omega + \kappa/2, \quad (51)$$

is satisfied, and the equality holds only at the Lindblad resonance points (for details see, e. g., Binney & Tremaine 2008). Also, at a certain radius R , and for a given pattern speed (Ω_p), the density wave will be *stable* if the corresponding $|s| (= m|\Omega_p - \Omega|/\kappa)$ is greater than the $|s|_{\text{cut-off}}$ value, say α , of the corresponding dispersion relation at that radius R (for detailed discussion see Binney & Tremaine 2008; Ghosh & Jog 2016). In other words, for obtaining a *stable* spiral density wave, with pattern speed Ω_p , the following condition needs to be satisfied

$$\Omega_p \geq \Omega + \alpha\kappa/2 \quad \text{or} \quad \Omega_p \leq \Omega - \alpha\kappa/2, \quad (52)$$

at radius R , depending on whether the radius R falls outside the CR or inside the CR. Therefore, by combining Eqs. (51) and (52), the allowed range of pattern speed (Ω_p) values for a stable, spiral density wave is

$$\Omega_p \in [\Omega - \kappa/2, \Omega - \alpha\kappa/2] \quad \text{or} \quad \Omega_p \in [\Omega + \alpha\kappa/2, \Omega + \kappa/2], \quad (53)$$

depending on whether the radius R is inside the corotation or outside the corotation. Now, as the value of α (or $|s|_{\text{cut-off}}$) increases with thickness, the allowed range of pattern speed values for a stable spiral density wave become progressively narrower. This is another finding of this work. Note that the inclusion of gas allows a larger range of allowed pattern speed values (Ghosh & Jog 2016). Thus, the effects of the gas and the disc thickness have an opposite effect on the range of pattern speed values corresponding to a stationary (non-evanescent) spiral density wave. This is further discussed in Sect. 4.2.

4.1.3. Radial group transport and effect on longevity of spiral density waves

Next, we study whether the radial group transport, and hence the longevity of a spiral density wave gets altered with the inclusion of finite thickness of the collisionless stellar disc. In classical density wave theory, the pattern speed (Ω_p) of the spiral arms is a free parameter (e. g., see Lin & Shu 1964, 1966). Observationally, the pattern speed of spiral density waves has been measured only for a few external galaxies (e. g., Fathi et al. 2007, 2009) apart from the Milky Way. Therefore, driven by purely theoretical interest, we treat the pattern speed (Ω_p) as a free parameter. For investigating the effect of disc thickness on the group velocity, we first assume the pattern speed to be $\Omega_p = 12.5 \text{ km s}^{-1}$, the same value as used in Toomre (1969). Also, we choose $Q = 1.1$ here, and vary β from 0 to 0.3. Now, using the definition of the dimensional quantity s as given earlier in this section (i.e., $|s| = 2(|\Omega_p - \Omega|/\kappa)$ and using Ω and κ values for a particular galaxy at a given radius, and a given value of Ω_p gives $|s|_{\text{obs}}$, the observed value of $|s|$. This is shown by the horizontal line in Fig. 1. Then, we compute the group velocity (v_g) at $R = 8.27 \text{ kpc}$, from the slopes of the corresponding dispersion relations (as shown in Fig. 1) with varying β values, the slope is obtained where the line $|s|_{\text{obs}}$ intersects the dispersion relation. The resulting values of the group velocity (v_g) and the time that one such wavepacket (of density wave) would take to travel a distance of 10 kpc are listed in Table 1. Before proceeding to interpreting dynamical effect of thickness on the group velocity, the location where the slopes are being calculated, merits a discussion. For an assumed Ω_p value and the values of Ω , and κ (set by the underlying mass distribution), the corresponding $|s|_{\text{obs}}$ would intersect the dispersion relations at two points: one at the long wavelength branch (lower x value), and another at a short wavelength branch (higher x value). For a given Ω_p value, we always calculate the group velocity in the short wavelength branch regime, as the WKB approximation works better there (for details, see Binney & Tremaine 2008).

Table 1. Group velocity for one-component stellar disc (with $Q = 1.1$) for various thickness values, calculated at $R = 8.27 \text{ kpc}$.

Ω_p ($\text{km s}^{-1} \text{ kpc}^{-1}$)	$ s _{\text{obs}}$	β	ds/dx	v_g (km s^{-1})	Time to travel 10 kpc (Gyr)
10	0.92	0	0.032	1.3	7.5
		0.1	0.04	1.62	6.03
		0.2	0.045	1.83	5.3
		0.25	0.047	1.91	5.1
		0.3	0.05	2.03	4.8
12.5	0.8	0	0.107	4.34	2.25
		0.1	0.123	5	1.95
		0.2	0.137	5.56	1.75
		0.25	0.142	5.77	1.69
		0.3	0.143	5.81	1.68
15	0.68	0	0.181	7.35	1.32
		0.1	0.199	8.1	1.2
		0.2	0.203	8.25	1.18
		0.25	0.204	8.29	1.17
		0.3	0.205	8.3	1.16

From Table 1, it is clearly seen that for $\Omega_p = 12.5 \text{ km s}^{-1} \text{ kpc}^{-1}$ and $Q = 1.1$, the value of the group velocity increases steadily with increasing disc thickness (β). As the β value changes from 0 to 0.3, the group velocity (v_g) increases by ~ 35 per cent. This implies that a wavepacket would take

less time to reach the centre of the disc (and get absorbed eventually) for a disc with finite thickness when compared to that of an infinitesimally-thin disc. In other words, a spiral density wave would survive for a lesser time for a stellar disc with finite thickness when compared to an infinitesimally-thin stellar disc. Next, we choose $\Omega_p = 10 \text{ km s}^{-1} \text{ kpc}^{-1}$, and $15 \text{ km s}^{-1} \text{ kpc}^{-1}$, and recalculate the variation of the group velocity with changing disc thickness. Here also we choose $Q = 1.1$. The corresponding results are also given in Table 1. We find that, for these pattern speed values, the group velocity increases with the disc thickness, similar to the case of $\Omega_p = 12.5 \text{ km s}^{-1} \text{ kpc}^{-1}$. However, the amount by which the group velocity changes, varies with the assumed pattern speed values. To elaborate, the group velocity increases by ~ 56 percent for $\Omega_p = 10 \text{ km s}^{-1} \text{ kpc}^{-1}$ whereas the group velocity increases by ~ 13 percent for $\Omega_p = 15 \text{ km s}^{-1} \text{ kpc}^{-1}$, once the thickness (β) is increased from 0 to 0.3. We also consider a higher Toomre Q value, namely, $Q = 1.5$ and study the variation of the group velocity with disc thickness. For the sake of brevity, the detailed variations in the group velocity values are not shown here. However, we find that, for an $Q = 1.5$, and $\Omega_p = 12.5 \text{ km s}^{-1} \text{ kpc}^{-1}$, the corresponding group velocity (v_g) increases by ~ 16 per cent for an increase in thickness from $\beta = 0$ to $\beta = 0.3$, as compared to ~ 35 per cent for $Q = 1.1$ obtained earlier.

We note that the measured group velocity is critically dependent on the location where the slope is being measured along the dispersion relation. Nevertheless, an increment in the group velocity value with the increasing disc thickness is seen to be a generic phenomenon, as shown here. Lastly, we point out that for the one-component stellar disc case, we could not explore a higher Toomre Q value and/or a higher pattern speed value, because for these cases, the measured $|s|_{\text{obs}}$ value is found to be lower than the $|s|_{\text{cut-off}}$ value. Consequently, the $|s|_{\text{obs}}$ does not intersect the corresponding dispersion relation. In other words, for higher Toomre Q values, and a higher pattern speed value, e.g., $\Omega_p = 18 \text{ km s}^{-1} \text{ kpc}^{-1}$ does not admit a real solution in k (or equivalently, x), and so we could not calculate the group velocity using Eq. (49). We will explore this parameter regime in the next section where the interstellar gas is taken into account.

4.1.4. Radial variation of the group transport

So far, we have calculated the group velocity of a typical wavepacket, made of density wave, at a certain radius, say R , to study the effect of the finite thickness of a stellar disc on the longevity of the spiral density wave. We have so far considered the group transport at the solar neighbourhood $R = 8.27 \text{ kpc}$. However, in reality, any spiral arm in a disc galaxy has a finite radial extent. Here, we study how the group velocity of a wavepacket changes at different radii for different thickness, and consequently how this affects the longevity of the spiral density wave.

We mention that, for an assumed flat rotation curve in the outer disc region, as done here, the values of κ and Ω will change at different radial locations. Therefore, for an assumed value of Ω_p which remains constant with respect to radius, the corresponding $|s|_{\text{obs}}$ value would change at different radial location, so would the x values where the $|s|_{\text{obs}}$ cuts the local dispersion relation. To evaluate this, we first take $\Omega_p = 12.5 \text{ km s}^{-1} \text{ kpc}^{-1}$ and $Q = 1.1$ (same as Table 1 which was done for $R = 8.27 \text{ kpc}$), and redo the group velocity calculation at $R = 6.27 \text{ kpc}$, $R = 7.27 \text{ kpc}$, and $R = 9.27 \text{ kpc}$. The results are given in Table 2. From Table 2, it is clearly seen that at three different radial locations we considered here, the variation of the finite thickness

from $\beta = 0$ to $\beta = 0.3$, leads to a monotonic increase of the group velocity of the density wavepacket. To express it more quantitatively, at $R = 6.27 \text{ kpc}$, the group velocity increases by ~ 66.2 percent when β is varied from 0 to 0.3 whereas at $R = 7.27 \text{ kpc}$, and $R = 9.27 \text{ kpc}$, the corresponding group velocity increases by ~ 49.8 and ~ 23.1 percent, respectively (for the same β variation). This trend is in concordance with that seen at $R = 8.27 \text{ kpc}$ (see Table 1). In other words, the finite thickness has a similar (qualitative) effect on the group velocity as well as the longevity of spiral density waves. We checked this trend for the other considered pattern values, namely, $\Omega_p = 15 \text{ km s}^{-1} \text{ kpc}^{-1}$, and $\Omega_p = 10 \text{ km s}^{-1} \text{ kpc}^{-1}$ as well. We found a qualitative trend in the results similar to what is seen for $\Omega_p = 12.5 \text{ km s}^{-1} \text{ kpc}^{-1}$, as long as the dispersion relation admits a real solution in x in the short wavelength branch for the corresponding $|s|_{\text{obs}}$ value (for details, see previous section). For brevity they are not shown here. To conclude, the finite thickness of the stellar disc has a similar quenching effect on the longevity of spiral density waves at different radial locations (covering the radial extent of spirals).

Table 2. Radial variation of group velocity for one-component stellar disc (with $Q = 1.1$, $\Omega_p = 12.5 \text{ km s}^{-1} \text{ kpc}^{-1}$), calculated at three radial locations.

R (kpc)	$ s _{\text{obs}}$	β	ds/dx	v_g (km s^{-1})	Time to travel 10 kpc (Gyr)
6.27	0.94	0	0.021	1.14	8.5
		0.1	0.027	1.46	6.7
		0.2	0.032	1.71	5.7
		0.25	0.034	1.82	5.35
		0.3	0.035	1.9	5.1
7.27	0.87	0	0.06	2.8	3.5
		0.1	0.074	3.42	2.85
		0.2	0.083	3.8	2.56
		0.25	0.086	3.9	2.45
		0.3	0.09	4.2	2.32
9.27	0.72	0	0.156	5.6	1.73
		0.1	0.178	6.4	1.51
		0.2	0.184	6.7	1.45
		0.25	0.188	6.8	1.43
		0.3	0.192	6.9	1.41

4.2. Effect of finite height on two-component star-gas system

In the earlier section, we show that the inclusion of finite thickness of the stellar disc makes it more stable against the non-axisymmetric perturbations, and increases the group velocity of a wavepacket, thereby decreasing the longevity of the spiral density wave. Further, Ghosh & Jog (2015) showed that for a gravitationally-coupled star-gas system where both the stellar and the gas discs are *infinitesimally-thin*, the inclusion of gas helps the spiral density waves to sustain for a longer time. Therefore, it is natural to investigate how the longevity of the spiral density wave is affected in a stars plus gas system with finite disc thickness.

To achieve that, first we calculate the dispersion relation (Eq. (46)) for the gravitationally-coupled star-gas system for different thickness of stellar disc (β_s) while assuming $Q_s = 1.5$, $Q_g = 1.3$, and taking two values of ϵ , namely, 0.15, and 0.2. We mention that, the thickness of the gas disc (β_g) is kept fixed at 0.1 throughout this paper, unless stated otherwise. The resulting dispersion relations are shown in Fig. 3. A visual inspection

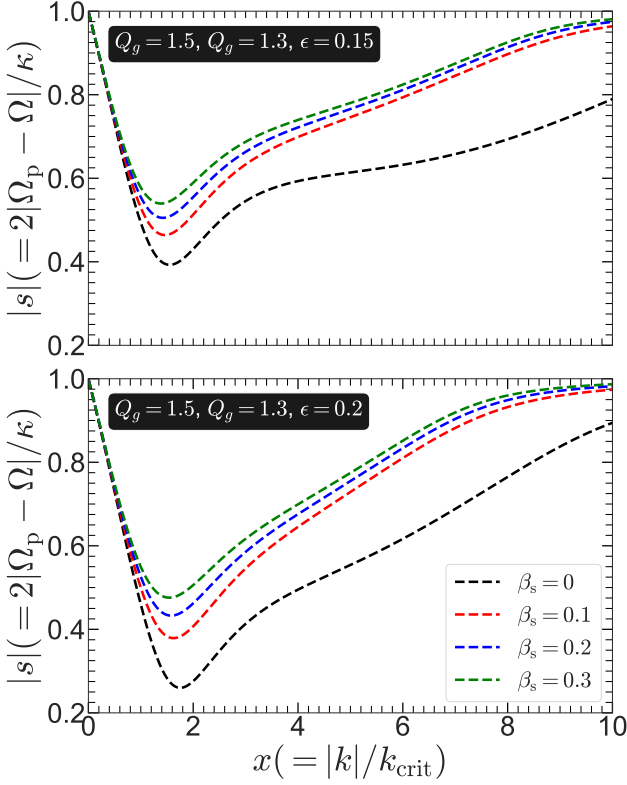


Fig. 3. Dispersion relations for the two-component stars plus gas system with finite thickness (Eq. (46)) are shown for $Q_s = 1.5$, $Q_g = 1.3$, and for different gas-fractions: $\epsilon = 0.15$ (top panel), $\epsilon = 0.2$ (bottom panel). The thickness of the stellar disc (β_s) is varied from 0.1 to 0.3, whereas the thickness of the gas disc (β_g) is kept fixed at 0.1 throughout all cases shown here. For comparison, the corresponding dispersion relation for the zero-thickness stars plus gas system is also shown (black dashed line).

reveals two broad trends, namely, for a fixed set of three values (Q_s , Q_g , ϵ), the value of $|s|_{\text{cut-off}}$ increases monotonically with the increase of thickness of the stellar disc. This trend is consistent with the findings for the one-component stellar disc. However, we notice that, with increasing gas fraction (ϵ), the increment in the $|s|_{\text{cut-off}}$ value with thickness, is less (compare top and bottom panels of Fig. 3). Secondly, the dispersion relation in the short-wavelength branch become increasingly flat with the increase of disc thickness, when compared with the same for the infinitesimally-thin star-gas system. This holds true for both the gas-fraction values considered here.

4.2.1. Disc stability against spiral waves, and allowed pattern speed values

In order to probe the joint effect of the disc thickness and the inclusion of gas on the variation of $|s|_{\text{cut-off}}$ values, we systematically calculate the relevant dispersion relations (using Eq. (46)) for a wide range of Q_s , Q_g , β_s , and ϵ . Then we compute the corresponding $|s|_{\text{cut-off}}$ values. The resulting variation of $|s|_{\text{cut-off}}$ values are shown in Fig. 4. Fig. 4 clearly demonstrates the generic trend that, for a fixed value of (Q_s , Q_g , ϵ), the $|s|_{\text{cut-off}}$ increases monotonically while the disc thickness (β_s) is varied from 0 to 0.5. However, the variation in the $|s|_{\text{cut-off}}$ values is more for a

lower Q_s value (say 1.2) when compared with a higher Q_s value (say, ~ 2). These findings are in compliance with the earlier finding for the one-component stellar disc. Next, we study how the variation in the $|s|_{\text{cut-off}}$ values with thickness, gets affected by the inclusion of the interstellar gas. We find that, for a fixed value of (Q_g , β_s), the $|s|_{\text{cut-off}}$ value for a higher gas-fraction (ϵ) is always lower when compared with the same for a lower gas-fraction (compare top and bottom panels of Fig. 4). This trend holds true for the whole range of Q_s and Q_g values considered here, although the trend is more prominent for the smaller values of Q_s . The physical reason behind this trend is when more gas present in the system (a lower Q_g value and a higher ϵ value), the destabilising effect of the interstellar gas wins over the stabilising effect of the finite thickness. This is particularly true when the Q_s and Q_g values are smaller (say close to 1) as the self-gravity of the stars-gas system would be important to determine the dynamical state of the system. Thus, the net stability of the gravitationally-coupled stars plus gas system is determined by the joint (mutually opposite) effects of the interstellar gas and the finite disc thickness. Nevertheless, the destabilising effect of the interstellar gas gets reduced (at least, partially) by the stabilising effect of the finite disc thickness in all cases shown here. Thus, the net range of allowed pattern speed values is higher for a two-component, finite height disc than a stars-alone, thin disk; but less than the range allowed for a two-component, thin disc.

4.2.2. Radial Group transport and effect on longevity of spiral waves

Finally, we turn to probe the joint effects of the disc finite thickness and the interstellar gas on the group velocity of the spiral density wave in a gravitationally-coupled stars-gas system. For the sake of theoretical interest, we choose a smaller value of Q_s , say 1.3. Also, for the moment, we treat Q_s and ϵ as free parameters, and Q_g is set by these two values via the relation $Q_g = (0.306Q_s)(1 - \epsilon)/\epsilon$ (for details see Ghosh & Jog 2015). Later, we will relax this constraint and will treat all three parameters, namely, Q_s , Q_g , and ϵ as free parameters while studying the group velocity.

To study how the group velocity changes, first we assume a $\Omega_p = 12.5 \text{ km s}^{-1} \text{ kpc}^{-1}$ which in turn, gives $|s|_{\text{obs}} = 0.8$ at $R = 8.27 \text{ kpc}$. Then we compute the group velocity from the slopes of the dispersion relations (Eq. (46)) for $Q_s = 1.3$ and $\beta_g = 0.1$ while varying the gas-fraction (ϵ) from 0.1 to 0.25, and disc thickness (β_s) from 0 to 0.3. The resulting variations of the slopes and the group velocity values are listed in Table 3. As evident from Table 3, the value of the group velocity increases with the increase of disc thickness, and this trend holds true for all values of gas-fraction considered here. However, there is subtle change with the increasing gas-fraction. To elaborate, when the gas-fraction is assumed to be 0.1, the group velocity increases by ~ 35 percent for a variation of 0 – 0.3 in the β values. However, for a higher gas-fraction value (say $\epsilon = 0.2$), the group velocity increases only by ~ 12 percent for the same variation of β values from 0 to 0.3. Further, when we choose an even higher value of gas-fraction (say, $\epsilon = 0.25$), we find a negligible increase in the group velocity (~ 2 percent) when we vary β from 0 to 0.3. The physical reason is as we choose progressively lower values of Q_g and higher values of ϵ , the overwhelming effect of the interstellar gas in decreasing the group velocity wins over the opposite effect of disc thickness on the group velocity values. In other words, when the self-gravity, and the low dispersion of interstellar gas dominates over the reduction in the self-gravity

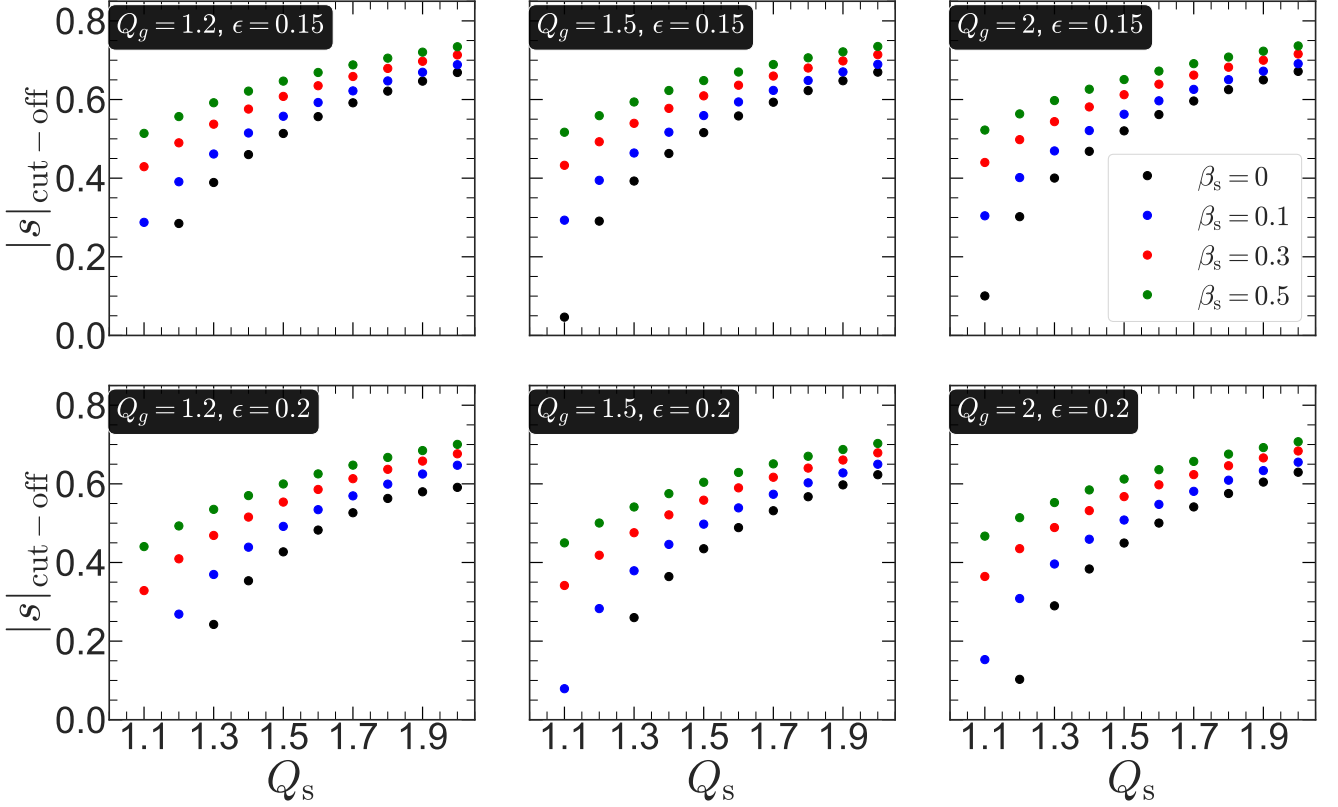


Fig. 4. Two-component stars plus gas system : Variation of the $|s|_{\text{cut-off}}$ values as a function of Toomre Q parameter for the stellar disc (Q_s) are shown for different stellar disc thickness (β_s), and for various Toomre Q parameter for the gas disc (Q_g), and gas-fraction (ϵ). The thickness of the gas disc (β_g) is kept fixed at 0.1 throughout all the cases shown here.

due to the finite thickness, the group velocity of a wavepacket, made of spiral density waves, is predominantly set by the effect of the interstellar gas. Next, we choose a higher pattern speed value, namely, $\Omega_p = 15 \text{ km s}^{-1} \text{ kpc}^{-1}$ which in turn, produces $|s|_{\text{obs}} = 0.68 R = 8.27 \text{ kpc}$. Then, we study how the group velocity changes as we vary simultaneously the gas-fraction, and the disc finite thickness. We find that, when $\epsilon = 0.1$, the group velocity increases by ~ 20 percent when the disc thickness is increased from 0 to 0.3. However, when the gas-fraction is changed to a higher value (say $\epsilon = 0.2$), the group velocity increases only by ~ 14 percent when β_s is varied from 0 to 0.3. This trend is similar to what we found for the $\Omega_p = 12.5 \text{ km s}^{-1} \text{ kpc}^{-1}$. Thus, the change in group velocity in presence of the disc thickness and the interstellar gas is a complex process, as these two physical factors have opposite effect on the group velocity. The net change in the group velocity is set by the relative dominance of the effects of the interstellar gas and the disc thickness.

To study further the net effect of the interstellar gas and the disc thickness where the parameters Q_s , Q_g , and ϵ are treated as free parameters (unlike the previous case), we choose a case where $Q_s = 1.3$, and $Q_g = 1.3$. For these assumed parameters, and for $\epsilon = 0.2$ and $\Omega_p = 15 \text{ km s}^{-1} \text{ kpc}^{-1}$, the group velocity increases by ~ 25 percent when β_s is varied from 0 to 0.3. This trend further demonstrate the mutual interplay of the (opposite) effects induced by the interstellar gas and the disc finite thickness. Lastly, we assume an even higher value of the pattern speed, namely,

Table 3. Group velocity for two-component star-gas system (with $Q_s = 1.3$) for various thickness values, calculated at $R = 8.27 \text{ kpc}$.

Ω_p (km s^{-1} kpc^{-1})	$ s _{\text{obs}}$	ϵ	β	ds/dx	v_g (km s^{-1})	Time to travel 10 kpc (Gyr)
12.5	0.8	0.1	0	0.081	3.3	2.95
			0.1	0.1	4.1	2.37
			0.2	0.104	4.2	2.32
			0.3	0.11	4.5	2.16
		0.15	0	0.067	2.72	3.58
			0.1	0.082	3.35	2.9
			0.2	0.083	3.4	2.86
			0.3	0.084	3.41	2.85
		0.2	0	0.074	3	3.24
			0.1	0.083	3.37	2.89
			0.2	0.0832	3.38	2.88
			0.3	0.0833	3.39	2.87
		0.25	0	-	-	-
			0.1	0.093	3.4	2.86
			0.2	0.095	3.42	2.84
			0.3	0.095	3.42	2.84

* The Toomre Q for gas disc (Q_g) is set by the values of Q_s and ϵ , for details see text. The thickness of the gas disc β_g is fixed at 0.1 for all cases.

$\Omega_p = 18 \text{ km s}^{-1} \text{ kpc}^{-1}$ which in turn, yields an $|s|_{\text{obs}} = 0.53$. For the current assumed parameter space (Q_s , Q_g , ϵ , β_s), it is possi-

ble to obtain a real solution in k (or alternatively, in x) for the $\Omega_p = 18 \text{ km s}^{-1} \text{ kpc}^{-1}$; thereby allowing us to probe the mutual effect of the gas and the thickness for a realistic value (or close to observationally reported values) of the Ω_p . Here also, we find the same trend in the change of the group velocity value as we increase the value of β_s . More quantitatively, when $\epsilon = 0.2$, the group velocity increases by ~ 11 per cent as we vary β_s from 0 to 0.3. However, the change in the group velocity is found to be negligible when ϵ is set to 0.25 while β_s is varied by a same amount as previous case. This further accentuates the complex mutual interplay of the opposite effects of the disc thickness and the interstellar gas on the resulting group velocity values.

Lastly, we explore the mutual effect of the disc thickness and the interstellar gas for some higher values of Q_s while varying the thickness of the stellar disc up to ~ 400 pc (equivalently, $\beta_s \sim 0.5$). This is close to the observed values of the disc thickness in the external galaxies (e. g., see de Grijs & Peletier 1997). For that, we first choose $Q_s = 1.6$, $Q_g = 1.5$, and $\epsilon = 0.2$, and then vary the disc thickness (β_s) from 0 to 0.5. We find that, for this chosen set of values for (Q_s , Q_g , ϵ), and for an assumed Ω_p of $15 \text{ km s}^{-1} \text{ kpc}^{-1}$, the group velocity increases monotonically with increasing disc thickness. We estimate that, for a variation of the disc thickness from 0 to 0.5, the group velocity increases by ~ 37 per cent. Further, we choose another set of values for (Q_s , Q_g , ϵ), namely, $Q_s = 2$, $Q_g = 2$, and $\epsilon = 0.2$. This set of chosen values is typical for the outer regions of the discs of Magellanic-type irregular galaxies where the gas fractions are high (e. g., see Gallagher & Hunter 1984; Jog 1992). We then choose a $\Omega_p = 12.5 \text{ km s}^{-1} \text{ kpc}^{-1}$, and vary the disc thickness from 0 to 0.5. We find that, for this case, the group velocity increases by ~ 13 percent as the disc thickness is varied from 0 to 0.5. Note that, for this case, we could not use a higher pattern speed value, say $\Omega_p = 15 \text{ km s}^{-1} \text{ kpc}^{-1}$ or higher as the group velocity approach cannot be applied here. The reason is, the $|s|_{\text{obs}}$ values corresponding to these higher pattern speed values are almost always less than the $|s|_{\text{cut-off}}$ values obtained from the dispersion relations corresponding to $Q_s = 2$, $Q_g = 2$, and $\epsilon = 0.2$, and $\beta_s = 0.2 - 0.5$.

4.2.3. Coverage on the parameter space

Thus, to conclude, we study the joint effect of the disc thickness and the interstellar gas on the stability of the disc against non-axisymmetric perturbations as well as on the longevity of the $m = 2$ spiral density waves. By exploring a range of parameter space, we demonstrate the complex nature of the mutually opposite effect of the disc thickness and the interstellar gas. We mention that, while studying this mutually opposite effect on the longevity of the spiral density wave, we could not carry out a systematic search in the parameter space, unlike the case of disc stability (or equivalently, the variation of $|s|_{\text{cut-off}}$). The reasons are as follows: first, the group velocity is obtained using the slope of the local dispersion relation graphically (as in Toomre 1969). Although this approach allows us to calculate the group velocity conveniently, this is a non-robust procedure (for details, see Toomre 1969; Ghosh & Jog 2015). The slope depends critically on the exact location of x where the $|s|_{\text{obs}}$ (corresponding to a Ω_p value) intersects the dispersion relation. In other words, it is a local value. Secondly, for a two-component system, the dispersion relation is a fourth-order polynomial (e.g. Jog & Solomon 1984). Thus for certain choice of parameters, if the $|s|_{\text{obs}}$ intersects the dispersion relation in the region of high x that falls in the region of second minimum, the slope would tend to flatten regardless

of the fact whether or not the solution in x , corresponding to that $|s|_{\text{obs}}$ value, is real or imaginary. Hence, while normally a higher β or thickness leads to a steeper slope, in such cases the flattening effect due to the k^4 behaviour may dominate and hence one may get a smaller slope for higher β , and hence leading to a smaller value of the group velocity. This is opposite to the typical dependence on disc thickness as shown above where a higher β was shown to result in a higher group velocity. In such cases, the effect of disc thickness would not oppose, instead it would show a similar trend to the effect of gas. This complex, mixed behaviour is more likely to be seen at high gas fraction (see Jog & Solomon 1984) or high $|s|_{\text{obs}}$. This could contribute to a diverse and complex dynamical behaviour, and hence the results obtained from varying the β parameter for a fixed set of (Q_s , Q_g , ϵ) values have to be interpreted with caution.

Also, so far we kept the thickness of the gas disc, $\beta_g = 0.1$ while calculating the dispersion relations for a two-component stars-plus-gas system. Using the k_{crit} value mentioned in section 3.1, this reduces to a $h_g \sim 70$ pc which is typical scale-height for the molecular hydrogen gas (e.g., Scoville & Sanders 1987). On the other hand, neutral hydrogen (H I) shows a typical value for the scale-height as ~ 150 pc (e.g., Lockman 1984) which corresponds to $\beta_g = 0.2$. Here, we briefly state what happens to the findings mentioned above when we set $\beta_g = 0.2$ instead of $\beta_g = 0.1$. We choose $Q_s = 1.3$, $Q_g = 1.3$, and $\epsilon = 0.2$, a case already explored in section 4.2. We then set $\beta_g = 0.2$, and vary β_s from 0-0.3, as before, to see the change in the radial group velocity corresponding to $\Omega_p = 15 \text{ km s}^{-1} \text{ kpc}^{-1}$, and $\Omega_p = 18 \text{ km s}^{-1} \text{ kpc}^{-1}$. For a fixed β_s and Ω_p values, the group velocity is seen to increase by $\sim 13 - 55$ per cent for $\beta_g = 0.2$ when compared with that for $\beta_g = 0.1$. This shows that finite thickness of the gas disc also increases the group velocity for the joint disc (and consequently decreases the longevity) in a similar fashion as the thickness of the stellar disc. We also considered a few other set of (Q_s , Q_g , ϵ) values to test this. We find the general trend of an increasing group velocity with an increase in thickness of the gas disc, for brevity we have not shown these cases here.

Nevertheless, we stress that, in general, the inclusion of thickness of the stellar disc and the interstellar gas have opposing effects on the disc stability against non-axisymmetric perturbations and the radial group transport, as illustrated in terms of the typical examples in this section (also see Table 3). In general, for the observed disc thickness and gas fraction values, as we have discussed in this section, the quenching effect of the height does not overcome (completely) the supporting role played by the gas, and hence a disc would still be expected to host non-axisymmetric features whose longevity will be supported by the gas.

4.2.4. Radial variation of the group transport for a two-component disc

As before, we study here the radial variation of the effect of finite thickness on the group velocity of a wavepacket, made of density wave, for a gravitationally-coupled stars-gas system. As before, we choose three radial locations at $R = 6.27 \text{ kpc}$, $R = 7.27 \text{ kpc}$, and $R = 9.27 \text{ kpc}$. Then we assume a $\Omega_p = 12.5 \text{ km s}^{-1} \text{ kpc}^{-1}$, and recalculate the group velocities for different disc thickness and the gas fraction values while choosing Q_s and Q_g values identical to what used for Table 3. Here also, we find a similar qualitative trend of mutually-opposing effects of the finite thickness and the interstellar gas on the group velocity as well

as the longevity of the spiral density waves. To elaborate, at $R = 6.27$ kpc, and for $\epsilon = 0.1$, and $\Omega_p = 12.5 \text{ km s}^{-1} \text{ kpc}^{-1}$, the group velocity increases by ~ 63.6 percent when β_s is varied from 0 to 0.3. As the gas fraction (ϵ) increases, the increment in the group velocity due to a variation of β from 0 to 0.3, starts to diminish monotonically. For $\epsilon = 0.2$, the corresponding increment in the group velocity becomes ~ 37.8 percent, and for $\epsilon = 0.25$, the increment in the group velocity becomes ~ 33.7 percent (for the same variation in β from 0 to 0.3). In other words, when the gas fraction becomes higher, the dynamical effect of the interstellar gas in supporting the spiral density wave starts to dominate over the quenching effect of the finite thickness. This trend is similar to what was shown for $R = 8.27$ kpc (see Table 3). We further checked for other Ω_p values as well as for other two radial locations considered here. We found that as long as the dispersion relation admits a real solution for x in the long wavelength branch for the corresponding $|s|_{\text{obs}}$ value, and the k^4 behaviour does not interfere in the locations where the group velocity is being calculated (for details, see the discussion in previous section), we obtained a similar qualitative effect of the finite thickness on the group velocity and on the longevity of the spiral density wave. For brevity, they are not shown here. Therefore, the finite thickness of the stellar disc has a similar quenching effect on the longevity of spiral density waves at different radial locations (covering the radial extent of spirals) for the gravitationally-coupled two-component disc as well.

5. Discussion

Here, we discuss a couple of points relevant for this work.

- At large values of scale height, its effect begins to dominate the effect of gas, hence the net effect is to increase the group velocity which would lead to a shorter lifetime of the density wave. A typical galaxy is known to show a flaring stellar disc as shown observationally by de Grijs & Peletier (1997). This feature occurs naturally as shown by the theoretical modelling of a multi-component galactic disc (Narayan & Jog 2002a). The Milky Way stellar disc also shows flaring as seen observationally from several surveys, e.g., 2MASS (Momany et al. 2006), SEGUE (López-Corredoira & Molgó 2014), LAMOST (Wang et al. 2018) as well as LAMOST plus Gaia (Yu et al. 2021). Such flaring was explained by theoretical modelling of a multi-component disc (Narayan & Jog 2002b), especially for the outer Galaxy by Sarkar & Jog (2018). This could explain in a generic way why spiral features are rare in outer regions even though such regions tend to be gas-rich.
- The formulation presented here employs the linear perturbation theory. However, the growth of the spirals in a real galaxy can enter the non-linear regime as well. The study by D’Onghia et al. (2013) demonstrated that the non-linear response of the disc to the non-axisymmetric perturbations can alter the life-time of spiral instability in a disc galaxy. While the study presented here, clearly demonstrates the mutually-opposite effect of the interstellar gas and the disc thickness on the disc stability and persistence of spiral density wave, it will be worth pursuing this effect in numerical simulations of disc galaxies. Also, we mention that, here the spiral structure is modelled as a two-dimensional structure for simplicity, as is typically done. However, some of the recent self-consistent simulations of growth of the spirals in disc galaxies (e. g., see Debattista 2014; Ghosh et al. 2020) show that the spirals can well be vertically extended.

6. Conclusion

In summary, we investigated the dynamical impact of the disc thickness on the disc stability, and the longevity of the spiral density wave. For that, we derived the dispersion relations in the WKB approximation for a collisionless stellar disc with finite thickness as well as for a gravitationally coupled stars-plus-gas system with different thickness for the stars and the gas discs. The main findings are mentioned below.

- The inclusion of finite thickness effectively reduces the self-gravity of the disc which in turn makes the disc more stable against the non-axisymmetric perturbations. This result in case of a one-component stellar disc, holds true for the whole range of Toomre- Q parameter (1.2 – 2) and the disc thickness (~ 50 – 400 pc) considered in this work. This stabilising effect is more prominent for lower values of Toomre- Q where the self-gravity of the disc is more important.
- The stabilising effect of the finite disc thickness has consequences in setting up the allowed range of pattern speed values for which the system allows a non-evanescent spiral density wave. With increasing disc thickness, this allowed range of pattern speed values gets progressively narrower, especially for lower values of Toomre- Q parameter. For a joint stars-plus-gas system, the effect of gas is to increase the range of pattern speed values while the thickness has an opposite effect. Typically, the net range of allowed pattern speed values is larger for a two-component, finite height disc than a stars-alone, infinitesimally-thin disc.
- For a one-component stellar disc, the group velocity of a wavepacket increases monotonically with the increment of disc thickness, thereby implying a progressively shorter life-time for the spiral density wave. For the same change in disc thickness by ~ 250 pc, the reduction in the life-time can vary from ~ 10 – 60 per cent when compared to the case of an infinitesimally-thin stellar disc; and this reduction depends on the assumed pattern speed values and the Toomre- Q parameter. In a two-component system, as the gas fraction is increased, the increase in the group velocity caused by the effect of finite height is reduced. Hence the inclusion of gas opposes the reduction in lifetime arising due to the finite thickness.
- Even in the presence of the interstellar gas, the disc thickness tends to stabilise the two-component (stars-gas) system against the non-axisymmetric perturbation, and this holds true for the whole parameter space ($Q_s = 1.2$ – 2 , $Q_g = 1.2$ – 2 , $\epsilon \sim 0.10$ – 0.25) considered here. However, when the dynamical effect of gas is important (e.g., lower values of Q_g , and/or higher ϵ values), the stabilising effect of the disc thickness becomes minimal.
- The disc thickness tends to diminish the life-time of the spiral density waves, even when the gas is present. For the same change in disc thickness by ~ 400 pc, the amount of reduction in the life-time can vary from ~ 5 – 40 per cent when compared to an infinitesimally-thin stars-plus-gas system, depending on the assumed pattern speed and the Q_s , Q_g and gas-fraction (ϵ) values. However, for gas-rich systems ($\epsilon \geq 0.25$), the effect of finite disc thickness is shown to be negligible.

Thus, to conclude, we demonstrate in this paper that the interstellar gas and the disc thickness have an opposite dynamical effect on the disc instability and the persistence of spiral density waves. While the gas makes a galactic disc more susceptible against non-axisymmetric perturbations and helps the

spiral density wave to survive for a longer time-scale, the disc thickness influences the system in an opposite manner. Consequently, the net dynamical effect is set by the relative dominance of these two physical factors. For the broad range of parameter space we considered, the quenching effect of the height does not completely suppress the supporting role of the gas, and hence a disc would still be expected to host non-axisymmetric features whose longevity will be supported by the gas.

Acknowledgements

We thank the anonymous referee for useful comments which helped to improve this paper. C. J. thanks the DST, Government of India for support via a J.C. Bose fellowship (SB/S2/JCB-31/2014).

References

- Athanassoula, E. 2012, *MNRAS*, 426, L46
 Baba, J., Saitoh, T. R., & Wada, K. 2013, *ApJ*, 763, 46
 Binney, J. & Tremaine, S. 2008, *Galactic Dynamics: Second Edition* (Princeton University Press)
 Bournaud, F., Combes, F., Jog, C. J., & Puerari, I. 2005, *A&A*, 438, 507
 Burstein, D. 1979, *ApJ*, 234, 829
 Buta, R. J., Sheth, K., Regan, M., et al. 2010, *ApJS*, 190, 147
 Comerón, S., Elmegreen, B. G., Knapen, J. H., et al. 2011a, *ApJ*, 741, 28
 Comerón, S., Knapen, J. H., Sheth, K., et al. 2011b, *ApJ*, 729, 18
 Comerón, S., Salo, H., & Knapen, J. H. 2018, *A&A*, 610, A5
 de Grijs, R. & Peletier, R. F. 1997, *A&A*, 320, L21
 Debattista, V. P. 2014, *MNRAS*, 443, L1
 Dobbs, C. & Baba, J. 2014, *PASA*, 31, e035
 Dobbs, C. L., Theis, C., Pringle, J. E., & Bate, M. R. 2010, *MNRAS*, 403, 625
 D’Onghia, E., Vogelsberger, M., & Hernquist, L. 2013, *ApJ*, 766, 34
 Elmegreen, D. M. & Elmegreen, B. G. 2014, *ApJ*, 781, 11
 Elmegreen, D. M., Elmegreen, B. G., Yau, A., et al. 2011, *ApJ*, 737, 32
 Fathi, K., Beckman, J. E., Piñol-Ferrer, N., et al. 2009, *ApJ*, 704, 1657
 Fathi, K., Toonen, S., Falcón-Barroso, J., et al. 2007, *ApJ*, 667, L137
 Faure, C., Siebert, A., & Famaey, B. 2014, *MNRAS*, 440, 2564
 Gallagher, John S., I. & Hunter, D. A. 1984, *ARA&A*, 22, 37
 García de la Cruz, J., Martig, M., Minchev, I., & James, P. 2021, *MNRAS*, 501, 5105
 Gerhard, O. 2002, in *Astronomical Society of the Pacific Conference Series*, Vol. 273, *The Dynamics, Structure & History of Galaxies: A Workshop in Honour of Professor Ken Freeman*, ed. G. S. Da Costa, E. M. Sadler, & H. Jerjen, 73
 Ghosh, S., Debattista, V. P., & Khachatryan, T. 2020, *arXiv e-prints*, arXiv:2009.02343
 Ghosh, S. & Jog, C. J. 2015, *MNRAS*, 451, 1350
 Ghosh, S. & Jog, C. J. 2016, *MNRAS*, 459, 4057
 Ghosh, S. & Jog, C. J. 2018, *A&A*, 617, A47
 Ghosh, S., Saha, K., Jog, C. J., Combes, F., & Di Matteo, P. 2021, *arXiv e-prints*, arXiv:2105.05270
 Gillessen, S., Eisenhauer, F., Trippe, S., et al. 2009, *ApJ*, 692, 1075
 Goldreich, P. & Lynden-Bell, D. 1965, *MNRAS*, 130, 125
 Grand, R. J. J., Kawata, D., & Cropper, M. 2012, *MNRAS*, 426, 167
 Hodge, J. A., Smail, I., Walter, F., et al. 2019, *ApJ*, 876, 130
 Jog, C. J. 1992, *ApJ*, 390, 378
 Jog, C. J. 2014, *AJ*, 147, 132
 Jog, C. J. & Solomon, P. M. 1984, *ApJ*, 276, 114
 Julian, W. H. & Toomre, A. 1966, *ApJ*, 146, 810
 Jurić, M., Ivezić, Ž., Brooks, A., et al. 2008, *ApJ*, 673, 864
 Kruk, S. J., Lintott, C. J., Bamford, S. P., et al. 2018, *MNRAS*, 473, 4731
 Li, C., Zhao, G., Jia, Y., et al. 2019, *ApJ*, 871, 208
 Lighthill, M. J. 1965, *Journal of the Institute of Mathematics and Its Applications*, 1, 1
 Lin, C. C. & Shu, F. H. 1964, *ApJ*, 140, 646
 Lin, C. C. & Shu, F. H. 1966, *Proceedings of the National Academy of Science*, 55, 229
 Lockman, F. J. 1984, *ApJ*, 283, 90
 López-Corredoira, M. & Molgó, J. 2014, *A&A*, 567, A106
 Lynden-Bell, D. & Kalnajs, A. J. 1972, *MNRAS*, 157, 1
 Masset, F. & Tagger, M. 1997, *A&A*, 322, 442
 McMillan, P. J., Kordopatis, G., Kunder, A., et al. 2018, *MNRAS*, 477, 5279
 Mera, D., Chabrier, G., & Schaeffer, R. 1998, *A&A*, 330, 953
 Momany, Y., Zaggia, S., Gilmore, G., et al. 2006, *A&A*, 451, 515
 Narayan, C. A. & Jog, C. J. 2002a, *A&A*, 390, L35
 Narayan, C. A. & Jog, C. J. 2002b, *A&A*, 394, 89
 Rix, H.-W. & Zaritsky, D. 1995, *ApJ*, 447, 82
 Roškar, R., Debattista, V. P., Quinn, T. R., Stinson, G. S., & Wadsley, J. 2008, *ApJ*, 684, L79
 Saha, K. & Elmegreen, B. 2016, *ApJ*, 826, L21
 Salo, H., Laurikainen, E., Buta, R., & Knapen, J. H. 2010, *ApJ*, 715, L56
 Sarkar, S. & Jog, C. J. 2018, *A&A*, 617, A142
 Sarkar, S. & Jog, C. J. 2019, *A&A*, 628, A58
 Savchenko, S., Marchuk, A., Mosenkov, A., & Grishunin, K. 2020, *MNRAS*, 493, 390
 Schönrich, R. 2012, *MNRAS*, 427, 274
 Schönrich, R. & Binney, J. 2009, *MNRAS*, 396, 203
 Schönrich, R., Binney, J., & Dehnen, W. 2010, *MNRAS*, 403, 1829
 Schönrich, R., McMillan, P., & Eyer, L. 2019, *MNRAS*, 487, 3568
 Scoville, N. Z. & Sanders, D. B. 1987, *H₂ in the Galaxy*, ed. D. J. Hollenbach & J. Thronson, Harley A., Vol. 134, 21
 Sellwood, J. A. 2011, *MNRAS*, 410, 1637
 Sellwood, J. A. 2012, *ApJ*, 751, 44
 Sellwood, J. A. & Binney, J. J. 2002, *MNRAS*, 336, 785
 Sellwood, J. A. & Carlberg, R. G. 1984, *ApJ*, 282, 61
 Sellwood, J. A. & Carlberg, R. G. 2019, *MNRAS*, 489, 116
 Sellwood, J. A. & Lin, D. N. C. 1989, *MNRAS*, 240, 991
 Shu, F. H. 2016, *ARA&A*, 54, 667
 Toomre, A. 1964, *ApJ*, 139, 1217
 Toomre, A. 1969, *ApJ*, 158, 899
 Toomre, A. 1981, in *Structure and Evolution of Normal Galaxies*, ed. S. M. Fall & D. Lynden-Bell, 111–136
 Toomre, A. & Toomre, J. 1972, *ApJ*, 178, 623
 Tsikoudi, V. 1979, *ApJ*, 234, 842
 Wang, H.-F., Liu, C., Xu, Y., Wan, J.-C., & Deng, L. 2018, *MNRAS*, 478, 3367
 Weinberg, M. D. 1992, *ApJ*, 384, 81
 Whitham, G. B. 1960, *Journal of Fluid Mechanics*, 9, 347
 Willett, K. W., Galloway, M. A., Bamford, S. P., et al. 2017, *MNRAS*, 464, 4176
 Yoachim, P. & Dalcanton, J. J. 2006, *AJ*, 131, 226
 Yu, S.-Y., Ho, L. C., Barth, A. J., & Li, Z.-Y. 2018, *ApJ*, 862, 13
 Yu, Z., Li, J., Chen, B., et al. 2021, *ApJ*, 912, 106
 Zaritsky, D., Salo, H., Laurikainen, E., et al. 2013, *ApJ*, 772, 135

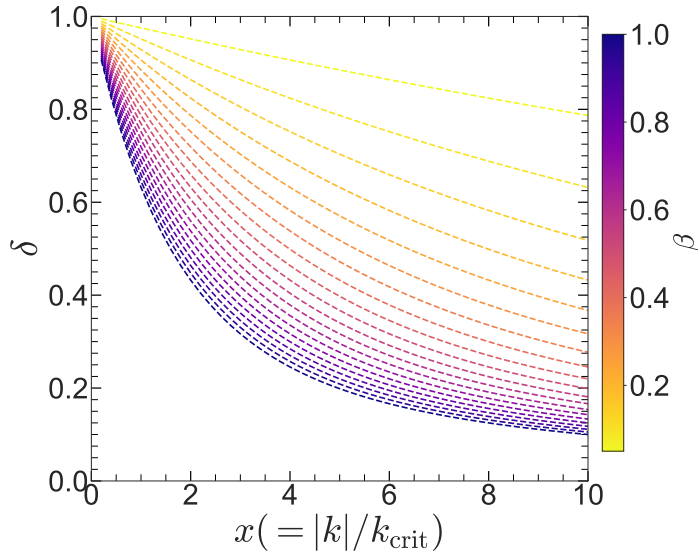


Fig. A.1. Variation of the reduction factor (δ) as a function of dimensionless wavenumber (x) are shown for different disc thickness (β values). The values of β are colour-coded here.

Appendix A: Behaviour of the Reduction factor

Fig. A.1 shows the variation of the reduction factor, δ (Eq. 43) with the dimensionless wavenumber x , for various disc thickness (or β values). The reduction due to the disc thickness becomes severe for larger values of disc thickness, as expected. Also, the reduction factor is seen to become progressively more important in the short-wavelength (large x) branch, as expected from the form of Eq. 43.